Table 1 Polarization ellipse characteristics for the three forms presented

		II		III	
Forms	I	+	−	Linear	Circular
E_{ox}	0.649	0.658	0.147	0.15	0.74
E_{oy}	0.855	0.868	0.112	0.58	0.74
δ, deg	−81.2	−81.2	98.8	0.0	90.0
a	0.868	0.880	0.150	0.595	1.096
b	0.632	0.641	0.109	0	1.096
α	52.8 deg	52.8 deg	37.2 deg	74.6 deg	—
ψ	75.6 deg	75.6 deg	165.6 deg	75.6 deg	—
χ	−36.1 deg	−36.1 deg	36.1 deg	0 deg	—
p	0.944	1.0	1.0	1	1

normalization of the Stokes vector elements. Estimates of errors caused by non-normal surfaces and careful CP alignment are in the order of 0.1 and 0.3%; respectively. The retardance angle error, determined by the manufacture, does need to be less than 2 deg. This largest source of error is based on the fact that the CP produces elliptical near-circular polarized energy and is component quality dependent (cost).

For the prototype instrument discussed in this note, preliminary test runs on sources of known polarization indicate the errors, as described by Holman,[18] in the magnitudes of the Stokes vector components are at the most in the order of ±10%. While this is not an enviable error band, it was deemed satisfactory based upon the cost of the instrument.

Conclusions

A prototype Stokesmeter [possibly the best commercially available Stokesmeter is offered by Gaertner Scientific Corporation for approximately $19,000 (LS-1 Stokesmeter)] was built to measure output intensities enabling the calculation of quantities associated with incident partially polarized radiation. An example was presented to demonstrate that the original partially polarized beam could be split in various ways into completely and unpolarized components.

Further, the mechanism enabling these measurements to be made consists primarily of a circular polarizer and a Geneva wheel. The other components are stock items or can be produced in any machine shop for a total cost of approximately $500.

Finally, a third degenerate form of the Stokes vector representing a partially polarized elliptical beam was presented. This form is novel in that the completely polarized components are of the most elementary forms (linear and circular) and the unpolarized portion indicates the insufficiencies of the incident beam to produce the elementary forms.

References

[1]Schmitt, J. M., Gandjbakhche, A. H., and Bonner, R. R., "Use of Polarized Light to Discriminate Short-Path Photons in a Multiply Scattering Medium," *Applied Optics*, Vol. 31, No. 30, 1992, pp. 6535–6546.

[2]Scholl, B., Stein, T., Neues, A., and Mertens, K., "In-Line Fiber Optic Polarimeter with a 99% Coupler," *Optical Engineering*, Vol. 34, No. 6, 1995, pp. 1669–1672.

[3]Krishnan, S., and Nordine, P. C., "Mueller-Matrix Ellipsometry Using the Division-of-Amplitude Photopolarimeter: A Study of Depolarization Effects," *Applied Optics*, Vol. 33, No. 19, 1994, pp. 4184–4192.

[4]Shindo, Y., "Application of Polarization Modulation Techniques in Polymer Science," *Optical Engineering*, Vol. 34, No. 12, 1995, pp. 3369–3384.

[5]Born, M., and Wolf, E., *Principles of Optics, Electromagnetic Theory of Propagation, Interference and Diffraction of Light*, 4th ed., Pergamon, New York, 1970, pp. 23–36, 554, 555.

[6]Bohren, C. F., and Huffman, D. R., *Absorption and Scattering of Light by Small Particles*, Wiley-Interscience, New York, 1983, pp. 44–53.

[7]Kliger, D. S., Lewis, J. W., and Randall, C. E., *Polarized Light in Optics and Spectroscopy*, Academic, New York, 1990, pp. 75–83, 92–102, 117–134.

[8]Collett, E., *Polarized Light, Fundamentals and Applications*, Marcel Dekker, New York, 1993, pp. 21–62.

[9]Kostinski, A. B., James, B. D., and Boerner, W.-M., "Optimal Reception of Partially Polarized Waves," *Journal of the Optical Society of America: A*, Vol. 5, No. 1, 1988, pp. 58–64.

[10]Bickel, W. S., and Bailey, W. M., "Stokes Vectors, Mueller Matrices, and Polarized Scattered Light," *American Journal of Physics*, Vol. 53, No. 5, 1985, pp. 468–478.

[11]*Mathematical and Physical Papers of G. G. Stokes: Vol. III*, Johnson Reprint Corp., New York, 1966, pp. 233–258.

[12]Chandrasekhar, S., "On the Radiative Equilibrium of a Stellar Atmosphere: XI," *Astrophysical Journal*, Vol. 104, No. 1, 1946, pp. 110–132.

[13]Chandrasekhar, S., "On the Radiative Equilibrium of a Stellar Atmosphere: XV," *Astrophysical Journal*, Vol. 105, No. 3, 1947, pp. 424–470.

[14]Soleillet, P., "Sur les Parametres Caracterisant la Polarisation Partielle, de la Lumiere dans les Phenomenes de Flurescence," *Annales de Physique*, Vol. 10, No. 12, 1929, pp. 23–97.

[15]Kent, C. V., and Lawson, J. J., "A Phototelectric Method for the Determination of Elliptically Polarized Light," *Journal of the Optical Society of America*, Vol. 27, No. 3, 1937, pp. 117–119.

[16]Azzam, R. M. A., and Lopez, A. G., "Accurate Calibration of the Four-Detector Photopolarimeter with Imperfect Polarizing Optical Elements," *Journal of the Optical Society of America: A*, Vol. 6, No. 10, 1989, pp. 1513–1521.

[17]Goldstem, D. H., and Chipman, R. A., "Error Analysis of a Mueller Matrix Polarimeter," *Journal of the Optical Society of America: A*, Vol. 7, No. 4, 1990, pp. 693–700.

[18]Holman, J. P., *Experimental Methods for Engineers*, 6th ed., McGraw–Hill, New York, 1994, p. 47.

Ignition of Propane–Air Mixture by Radiatively Heated Small Particles

Seung Wook Baek*
Korea Advanced Institute of Science and Technology, Taejon, 305-701, Republic of Korea

Introduction

FROM the view of fire safety, it is highly desirable to predict the critical conditions under which a reactive homogeneous or two-phase mixture ignites and produces a heat release. Ignition phenomena are usually governed by the heat

Received June 23, 1995; revision received Jan. 4, 1996; accepted for publication Jan. 9, 1996.

*Professor, Department of Aerospace Engineering. Member AIAA.

transfer modes of conduction, convection, and radiation, as well as by the inherent heat generation process pertaining to each mixture.

The thermal ignition of a single homogeneous medium, which contains absorbing and emitting gases, soot, and particles between isothermal and reflecting walls, was studied by Smith et al.[1] Baek[2] analyzed the thermal ignition of a two-phase mixture comprised of radiatively active combustible particles and air that is exposed to nonflaming conduction as well as to radiation.

A mixture state can be formulated such that solid inert particles are suspended in an ignitable premixed gas mixture. If this combustible mixture is in direct contact with a hot thermal source, the gas can be ignited by conductive heat transfer from the hot source. However, given a proper radiative thermal source, the gas is still inherently dangerous, although the gas is transparent to radiation and there is no thermal source in direct contact with the gas. This results from the fact that the particles absorb thermal radiation and are subsequently heated. The heated particles transfer energy to the gas, resulting in an exothermic reaction. Typical application of this scenario resides in a safety problem in coal mining and petroleum production industries. This type of potential hazard is briefly discussed in a previous paper using a suspension comprised of inert particles and hydrogen–air.[3]

As a further investigation, this study considers a mixture of propane, air, and inert particles. The ignition characteristics of propane–air and the effects of other important parameters, such as mixture equivalence ratio and incident radiation, are discussed. The fundamental physical features are considered through a simplified mathematical formulation so that a basic understanding of the induced ignition phenomena of a premixed combustible gas mixture is acquired.

Mathematical Formulations

Figure 1 schematically illustrates a two-phase mixture of inert aluminum oxide particles and propane–air contained between two transparent parallel walls. The total length of the mixture is L. At $x = 0$ and $x = L$, the mixture is subject to external radiation $q^+ = \sigma T_l^4$ and $q^- = \sigma T_r^4$, respectively, where T_r and T_l are the right-hand side (RHS) and left-hand side (LHS) blackbody radiative heat source temperatures. The mixture is uniformly distributed one dimensionally and remains quiescent. The volume occupied by the spherical particles is neglected in comparison with the gas suspension volume.

The species mass conservation equation for species i, where $i = 1$ to I, with I denoting the total number of species, is then

$$\rho_g \frac{\partial y_i}{\partial t} = \rho_g D \frac{\partial^2 y_i}{\partial x^2} + \omega_i \tag{1}$$

where t and x are the time and spatial coordinates, ρ_g is the gas density, y_i is the mass fraction for species i, and ω_i is the production rate for species i. The multicomponent diffusion coefficient is D.

Only a negligible amount of product gases, such as water vapor and carbon dioxide, are generated before ignition. Furthermore, the partial pressure of water vapor and carbon dioxide in atmosphere is 0.155 and 0.116 atm. Their total emittances for the conditions given are about 0.025 and 0.035, so that the effects of gas radiation by those species are neglected here. The energy equation for the gas phase then becomes

$$\rho_g C_g \frac{\partial T_g}{\partial t} = \lambda_g \frac{\partial^2 T_g}{\partial x^2} - nQ - \sum_{i=1}^{I} \Delta H_i \omega_i \tag{2}$$

T_g is the gas-phase temperature, and λ_g and C_g are the thermal conductivity and specific heat at constant pressure of the gas mixture, respectively. The enthalpy of formation for species i is ΔH_i. The particle number density is denoted by n. The heat transfer between the gas and a single particle is

$$Q = \pi D_c^2 h (T_g - T_c) \tag{3}$$

where D_c is the particle diameter and h is the convective heat transfer coefficient. Because the mixture of particles and propane–air is stagnant, the convective heat transfer coefficient h is estimated using

$$Nu = hD_c/\lambda_g = 2$$

To predict the precise ignition delay time of the propane–air mixture, an accurate estimation of total heat release for all of the species involved in Eq. (2) is needed. The chemical reaction model considers a total of 31 species (C_3H_8, O_2, OH, H, O, N_2, H_2, H_2O, HO_2, CO, CO_2, CH_4, CH_3, CH_2O, HCO, C_2H_6, C_2H_5, C_2H_4, C_2H_3, C_2H_2, CH_2CO, CH_2, CH, C_2H, HCCO, C_3H_7(I), C_3H_7(N), C_3H_6, CH_3HCO, H_2O_2, CH_3CO), and 123 elementary reaction steps. The reaction scheme and the corresponding rate constants used are ones in Djavdan et al.[4] The CHEMKIN subroutines[5] are exploited to calculate the reaction rates ω_i.

The inert particle properties are assumed to vary spatially as well as temporally. The particle property at a local position takes a value averaged over some neighborhood. From this point of view, the size of the neighborhood must be larger than the average spacing between particles. This averaging concept allows for a superposition of the solid phase computational domain over the gas phase one. The energy equation for the solid phase is

$$\sigma_c C_c \frac{\partial T_c}{\partial t} = nQ - \frac{\partial q_r}{\partial x} \tag{4}$$

where σ_c and C_c are the concentration and specific heat of solid particles, respectively; T_c is the particle temperature; and q_r is the net radiative heat flux that is expressed in terms of q^+ and q^- in the forward and backward directions, such that

$$q_r = q^+ - q^- \tag{5}$$

The governing equations for q^+ and q^- are derived using a two-flux gray radiation approximation. By integrating the equation of transfer for radiant intensity over the hemisphere, they are obtained as follows:

$$\frac{dq^+}{dx} = -2(a + s)q^+ + 2sq^- + 2a\sigma T_c^4 \tag{6}$$

$$\frac{dq^-}{dx} = 2(a + s)q^- - 2sq^+ - 2a\sigma T_c^4 \tag{7}$$

where a and s are the absorption and scattering coefficients of aluminum oxide particles.

For the previous formulations to be physically plausible, a model is necessary for the absorption coefficient for aluminum oxide particles. The extinction coefficient $(a + s)$ for the aluminum oxide particles is $0.25\pi n D_c^2 Q_R$ as given by Brewster.[6] But in this work this value is assigned to the absorption coefficient without scattering, i.e., $s = 0$ to examine the maximum ignitability of the gas mixture by aluminum oxide particles.

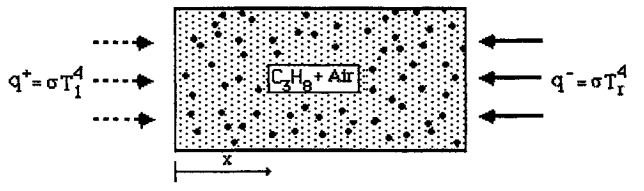

Fig. 1 Schematic diagram of physical system.

The Rosseland mean particle extinction efficiency Q_R is set to 1 for $10 < \pi D_c/\delta < 100$, where δ is wavelength.

The boundary conditions are $q^+(x = 0, t) = \sigma T_l^4$, $q^-(x = L, t) = \sigma T_r^4$. The dy_i/dx and dT_g/dx are all zero at $x = 0$ and L. The initial conditions are $T_g(x, 0) = T_c(x, 0) = 300$ K. The initial mass fraction y_i for species i is dependent upon the initial mixture equivalence ratio ϕ.

Because the species conservation Eq. (1), the energy Eq. (2) for the gas phase, and the thermal Eq. (4) for solid phase, with supplementary Eqs. (6) and (7) for the radiative heat fluxes are nonlinearly coupled to one another, a numerical method is adopted to solve them simultaneously. Equations (1) and (2) with given initial and Neumann boundary conditions are solved in dimensionless form by implementing an implicit, central difference scheme with a tridiagonal matrix solver. Then, the solutions are recast into dimensionless forms. The time step and spatial differencing used are 10^{-7} s and 5×10^{-3} m. No appreciable improvement in the solution was observed with more refinement in time step and spatial differencing.

Results and Discussion

Unless otherwise specified, all of the calculations are carried out for the following conditions: the equivalence ratio of the propane–air mixture is $\phi = 1$, the particle number density is $n = 10^9$ m^{-3}, the total length of the mixture is $L = 0.05$ m, the aluminum oxide particle diameter is $D_c = 100$ μm, and the external heat source temperature at $x = 0$ is $T_l = 0$ K.

The transient solution for both the gas mixture and particle temperature proceeds until ignition is detected. Figure 2 shows a temporal variation of particle and gas temperatures at $x = L$ for external blackbody heat source temperature $T_r = 2500$ K. Because there is no external heat source other than radiation, the particles initially warm up by way of absorption of radiation. The gas mixture is heated by the particles through conductive heat transfer, thereby creating a temperature difference between the two phases as seen in Fig. 2. As the ignition takes place, the gas temperature exceeds the particle temperature. The onset of ignition is, therefore, defined here as the time required for the two temperature curves to cross each other. According to this definition, the ignition delay time is 51.1 ms in the figure for the conditions given.

Spatially, the temperature of the radiatively active particles is higher than that of the gas mixture before the onset of ignition, as a result of the effects of radiation. Consequently, the radiation is found to play a considerable role in the rapid heating of the particles and resulting indirect ignition of gas mixture.

Using the definition of ignition mentioned previously, the ignition delays are plotted in Fig. 3 on both linear and logarithmic scales vs the inverse of the external source temperature. The ignition delay time increases with decreasing T_r and varies almost linearly on the logarithmic scale. This form of representation is typical of systems governed by an exothermic

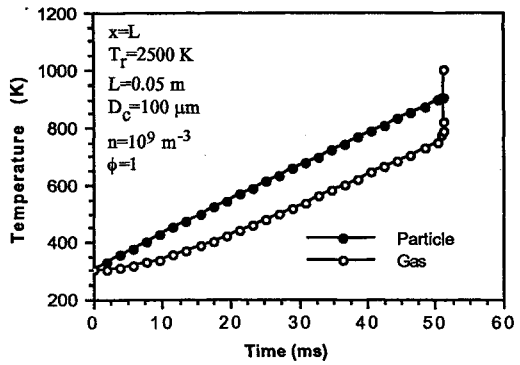

Fig. 2 Temporal variation of particle and gas mixture temperature at $x = 0.05$ m for $\phi = 1.0$, $L = 0.05$ m, $D_c = 100$ μm, $n = 10^9$ m^{-3}, $T_r = 2500$ K, and $Nu = 2$.

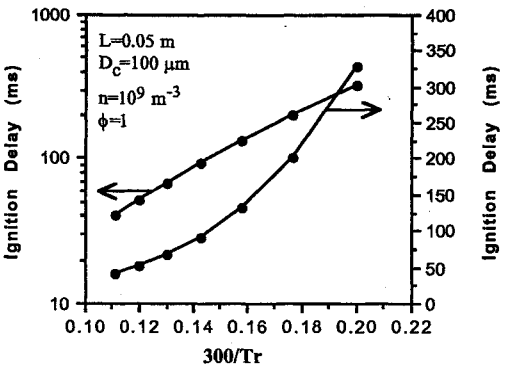

Fig. 3 Calculated ignition delays for $\phi = 1.0$, $L = 0.05$ m, $D_c = 100$ μm, $n = 10^9$ m^{-3}, $Nu = 2$, and $T_r = 1500$, 1700, 1900, 2100, 2300, 2500, and 2700 K.

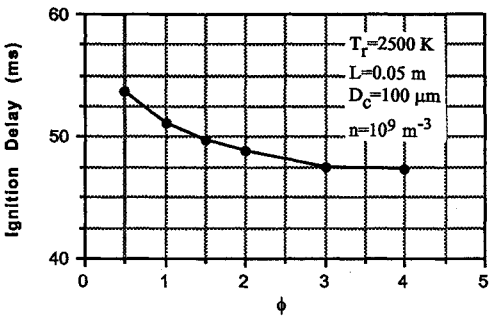

Fig. 4 Effect of the gas mixture equivalence ratio, ϕ on the ignition delays for $L = 0.05$ m, $D_c = 100$ μm, $n = 10^9$ m^{-3}, $T_r = 2500$ K, and $Nu = 2$.

reaction of the Arrhenius type, which is represented by the overall activation energy.

The effect of the equivalence ratio of the gas mixture on the ignition delay is shown in Fig. 4. In the range of $0.5 < \phi < 3$, the ignition delay decreases somewhat as ϕ increases, and then there is no obvious change, even if ϕ increases up to 4. Therefore, it is considered that the equivalence ratio has only a minor effect on the ignition delays for $0.5 < \phi < 4$.

When the particle number density decreases from $n = 10^{10}$ to 10^9 to 10^8 m^{-3} with fixed particle parameters, the absorption coefficient as well as the particle concentration decreases. Therefore, the radiation plays a smaller role, and the ignition delay increases from 37.9 to 51.1 to 142 ms as n decreases.

When T_l is increased from 0 to 1000 to 2000 K with a fixed value of $T_r = 2500$ K, the ignition delay decreases from 51.1 to 50.7 to 44.6 ms, respectively. Therefore, as long as the RHS external heat source is strong enough for ignition, the ignition delay seems to be comparatively less influenced by the change in the LHS external heat source for the optical thickness of 0.393.

Conclusions

In this study, time and spatially dependent results are obtained to study the indirect thermal ignition of combustible gases by inert particles. A one-dimensional geometry has been used together with a detailed chemical kinetics. The external thermal radiation originated from a blackbody source maintained a high temperature. The ignitable premixed gases were comprised of propane and air, and the inert aluminum oxide particles contained in the mixture are considered to absorb and emit radiation. Based on a standard two-flux radiation model, the parameters include the external radiation source temperature, mixture equivalence ratio, and particle number density. The numerical results revealed that the aluminum oxide particles heated by absorbing the radiant energy could ignite the propane–air mixture in less than 350 ms for the range of external blackbody temperature of $1500 < T_r < 2700$ K. There-

fore, the absorption of radiation by inert particles is found to play an important role in indirectly igniting combustible gases.

The change of particle number density at a fixed particle size also exerted a strong influence such that the smaller the particle number density, the longer the ignition delay. As the particle number density decreases, the radiation plays a smaller role, because the absorption coefficient decreases with a fixed particle size and the ignition delay increased.

Acknowledgments

Financial assistance from the Objective Research Fund of the Korea Science and Engineering Foundation is gratefully acknowledged. The author is also indebted to T. F. Smith, the Associate Editor, for his efforts in improving this manuscript.

References

[1]Smith, T. F., Byun, K. H., and Chen, L. D., "Effects of Radiative and Conductive Transfer on Thermal Ignition," *Combustion and Flame*, Vol. 73, No. 1, 1988, pp. 67–74.

[2]Baek, S. W., "Ignition of Particle in Slab Geometry," *Combustion and Flame*, Vol. 81, Nos. 3–4, 1990, pp. 366–377.

[3]Baek, S. W., "Ignition of Combustible Gases by Radiative Heating of Inert Particles," *Combustion and Flame*, Vol. 97, Nos. 3–4, 1994, pp. 418–422.

[4]Djavdan, E., Darabiha, N., Giovangigli, V., and Candel, S. M., "Strained Propane-Air Flames with Detailed and Reduced Kinetic Schemes," *Combustion Science and Technology*, Vol. 76, Nos. 3–4, 1991, pp. 287–309.

[5]Kee, R. J., Miller, J. A., and Jefferson, T. H., "CHEMKIN: A General-Purpose, Problem-Independent, Transportable, Fortran Chemical Kinetics Code Package," Sandia Rept. 80-8003, 1980.

[6]Brewster, M. Q., "Radiation-Stagnation Flow Model Aluminized Solid Rocket Motor Internal Insulator Heat Transfer," *Journal of Thermophysics and Heat Transfer*, Vol. 3, No. 2, 1989, pp. 132–139.

Effective Stagnant Thermal Conductivity of Wire Screens

C. T. Hsu,* K. W. Wong,† and P. Cheng‡
Hong Kong University of Science and Technology, Clear Water Bay, Kowloon, Hong Kong

Nomenclature

A	=	parameter of the wire screen in Eq. (1), d/w
a	=	length of the cross-sectional area of the bars in the x direction
B	=	parameter of the wire screen in Eq. (1), d/t
b	=	length of the cross-sectional area of the bars in the z direction
c	=	length of one side of the contact area
d	=	diameter of the wire
k_{ex}, k_{ey}, k_{ez}	=	effective thermal conductivities of the wire screens in the three principal directions
k_f	=	thermal conductivity of the fluid phase
k_s	=	thermal conductivity of the solid phase
l_x, l_y, l_z	=	spacing of wires in the x, y, and z directions, respectively
t	=	thickness of a layer of screen in Eq. (1)
w	=	opening of wires in Eq. (1)
α	=	empirical constant in Eq. (1)
γ_{ax}, γ_{ay}, γ_{bz}	=	a/l_x, a/l_y, and b/l_z, respectively
γ_c	=	c/a
λ	=	fluid/solid conductivity ratio

Received March 27, 1995; revision received Nov. 14, 1995; accepted for publication Nov. 20, 1995.

*Senior Lecturer, Department of Mechanical Engineering. Member AIAA.

†Research Assistant, Department of Mechanical Engineering. Member AIAA.

‡Professor and Head, Department of Mechanical Engineering. Senior Member AIAA.

I. Introduction

An accurate prediction of the effective thermal conductivity of wire screens saturated with fluids is needed for the design of heat pipes[1] and the regenerators of Stirling machines. Although Maxwell's analytical expression[2] for the thermal conductivity of a porous medium has been widely used for the design of fluid-saturated screen wicks in heat pipes,[1] it is known that this expression is inaccurate in comparison with experimental data. Alexander[3] obtained an empirical correlation equation for thermal conductivities of sintered layers of wire screens saturated with water and air. Van Sant and Malet[4] carried out an experiment to measure effective thermal conductivities of 100-mesh size of stainless steel screens and copper screens saturated with water, CH_3OH, CCl_3F, and air, respectively. Comparing Van Sant and Malet's[4] data with Maxwell's expression[2] and Alexander's correlation,[3] Chang[5] found that the former underpredicts the effective thermal conductivity at large solid/fluid thermal conductivity ratios, whereas the latter overpredicts the effective thermal conductivity substantially. Using an electric analogy, Chang[5] obtained the following algebraic expression for the effective thermal conductivity of wire screens in the direction perpendicular to the layers of wires

$$\frac{k_{ez}}{k_f} = \frac{1}{(1+A)^2}\left(\alpha^2 A\left\{\frac{\alpha A}{\alpha - \pi B(1-\lambda)/2} + \frac{2[1+A(1-\alpha)]}{\alpha - \pi B(1-\lambda)/4}\right\} + [1+A(1-\alpha)^2]\right) \tag{1}$$

In matching Eq. (1) with Van Sant and Malet's experimental data,[4] Chang[5] found that the value of α is approximately equal to unity. In this Note, we idealize the screens as alternate layers of parallel solid bars, and apply the lumped parameter method[6] to obtain algebraic expressions for the effective thermal conductivity of screens in three principal directions. The major difference between Chang's model[5] and the present model is that contact resistance between the wires will be taken into consideration in the present work. For the specific case of alternate layers of parallel and perpendicular bars of equal spacing, the predicted thermal conductivity in the direction perpendicular to the layers of screen is found in reasonably good agreement with Van Sant and Malet's experimental data.[4] In addition, we have obtained algebraic expressions for the thermal conductivity of wire screens in the direction parallel to the layers of wire screens that has not been considered previously.

II. Application of the Lumped Parameter Method

We now idealize a stack of wire screens as layers of parallel and perpendicular bars of rectangular cross sections laid on the x–y plane as shown in Fig. 1a. It is noted that the undulation effect of wires weaving into screens is neglected through this idealization. The bars parallel in the x direction are separated by a distance of l_y, having a rectangular cross section of $(a \times b)$ (see Fig. 1b). On the other hand, the bars parallel in the y direction are separated by a distance of l_x, having a cross section of $(a \times b)$. If the wire screens consist of circular wires of d, the circular wires will be approximated as square bars with an equivalent area $a \times a$, while the contact areas between the wires in the z direction will be approximated by small rectangular blocks with a square cross-sectional area of $c \times c$ (see Fig. 1). The length c of the contact area between two consecutive layers of screens is a parameter whose value depends on the loading stress during the packing of the